Modeling the climate response to a massive methane release from gas hydrates

Renssen, H.; Beets, C.J.; Fichefet, T.; Goosse, H.; Kroon, D.

published in
Paleoceanography
2004

DOI (link to publisher)
10.1029/2003PA000968

document version
Publisher's PDF, also known as Version of record

Modeling the climate response to a massive methane release from gas hydrates

H. Renssen and C. J. Beets
Faculty of Earth and Life Sciences, Vrije Universiteit Amsterdam, Amsterdam, Netherlands

T. Fichefet and H. Goosse
Institut d'Astronomie et de Géophysique Georges Lemaître, Université Catholique de Louvain, Louvain-la-Neuve, Belgium

D. Kroon
Faculty of Earth and Life Sciences, Vrije Universiteit Amsterdam, Amsterdam, Netherlands

Received 26 September 2003; revised 27 February 2004; accepted 17 March 2004; published 27 April 2004.

[1] The climate response to a massive release of methane from gas hydrates is simulated in two 2500-year-long numerical experiments performed with a three-dimensional, global coupled atmosphere-sea ice-ocean model of intermediate complexity. Two different equilibrium states were used as reference climates; the first state with preindustrial forcing conditions and the second state with a four times higher atmospheric CO_2 concentration. These climates were perturbed by prescribing a methane emission scenario equivalent to that computed for the Paleocene/Eocene thermal maximum (PETM; ~55.5 Ma), involving a sudden release of 1500 Gt of carbon into the atmosphere in 1000 years. In both cases, this produced rapid atmospheric warming (up to 10°C at high latitudes) and a reorganization of the global overturning ocean circulation. In the ocean, maximum warming (2–4°C) occurred at intermediate depths where methane hydrates are stored in the upper slope sediments, suggesting that further hydrate instability could result from the prescribed scenario. *INDEX TERMS:* 1620 Global Change: Climate dynamics (3309); 4255 Oceanography: General: Numerical modeling; 4267 Oceanography: General: Paleoceanography; 4532 Oceanography: Physical: General circulation; *KEYWORDS:* methane, climate model

Citation: Renssen, H., C. J. Beets, T. Fichefet, H. Goosse, and D. Kroon (2004), Modeling the climate response to a massive methane release from gas hydrates, *Paleoceanography*, *19*, PA2010, doi:10.1029/2003PA000968.

1. Introduction

[2] Catastrophic releases of methane gas from hydrates (clathrates) have been mentioned to be responsible for rapid climate changes in the past [e.g., *Dickens et al.*, 1995; *Kennett et al.*, 2002]. In the present climate, methane hydrates are stored along continental margins (i.e., at intermediate water depths, from 250 m to several thousand meters water depth), where they are stabilized by in situ water pressure and temperature fields. Methane hydrates may become unstable under influence of ocean warming or slope instability [*Buffet*, 2000; *Dickens*, 2001]. The estimated present-day reservoir of carbon stored in methane hydrates is about 10,000 Gt [*Kvenvolden*, 1988; *Buffet*, 2000], which is a substantial amount compared to 38,000 Gt carbon stored in the oceans, 2000 Gt in soils and plants, and 730 Gt in the atmosphere [*Prentice et al.*, 2001]. This implies that instability of these hydrates and the subsequent release of methane gas into the atmosphere could potentially cause strong climatic warming through an enhancement of the greenhouse effect.

[3] The Paleocene/Eocene thermal maximum (PETM, ~55.5 Ma) is a well-known example of a transient period with drastic climate change possibly due to massive releases of methane from hydrates [e.g., *Dickens et al.*, 1995, 1997]. In ocean cores from several locations (e.g., Caribbean, North Atlantic, subtropical South Atlantic, Weddell Sea, tropical Pacific), a −2.5 to −3‰ $\delta^{13}C$ excursion has been found in biogenic carbonate and organic matter, which is most likely caused by a release of 1500–2000 Gt of methane carbon within a few thousand years [*Dickens et al.*, 1995; *Bralower et al.*, 1997; *Bains et al.*, 1999; *Thomas et al.*, 1999, 2002]. This massive methane release had a profound effect on climate. Measurements of the oxygen isotope composition and Mg/Ca ratio of planktonic foraminifera indicate that oceanic surface temperatures increased abruptly by 1 to up to 8°C (depending on the location) coincident with the $\delta^{13}C$ excursion [e.g., *Thomas et al.*, 2002; *Zachos et al.*, 2003]. This is consistent with important amounts of carbon reaching the atmosphere and causing global warming through an enhanced greenhouse effect [*Dickens*, 2000; *Thomas et al.*, 2002]. The large amounts of methane carbon released also influenced the carbon chemistry of the ocean. The PETM interval sediments in all ocean cores show pronounced dissolution of carbonate.

[4] It has also been suggested that large temperature swings during the last glacial have been caused by abrupt releases of methane hydrates [e.g., *Nisbet*, 1990; *Kennett et al.*, 2000, 2002; *Hinrichs et al.*, 2003]. In this case, the methane releases could have been caused by sea level changes, triggering continental slope instability [*Rothwell*

0883-8305/04/2003PA000968$12.00

et al., 1998; *Nisbet and Piper*, 1998]. There is, however, still debate on the question to what extent glacial atmospheric methane variations originate from the decomposition of hydrates [e.g., *Brooks et al.*, 2000; *Dickens*, 2003]. Despite these uncertainties, there is some concern that the expected future global warming may lead to hydrate instability and thus to an enhanced emission of methane, imposing a strong positive feedback that would amplify anthropogenic warming [e.g., *Harvey and Zhen*, 1995; *Prather et al.*, 2001]. Accordingly, it is important to quantify the impact of such a methane hydrate scenario on the climate system.

[5] Numerical climate models have been used extensively to study the Paleocene-Eocene climate [e.g., *Sloan and Pollard*, 1998; *Peters and Sloan*, 2000; *Bice and Marotzke*, 2001, 2002; *Shellito et al.*, 2003]. For instance, *Schmidt and Shindell* [2003] (hereinafter referred to as SS03) used a two-dimensional (2-D) atmospheric chemistry model to estimate the effect of several methane hydrate release scenarios on atmospheric methane and carbon dioxide concentrations, taking the preindustrial climate as a reference state. These scenarios are based on the PETM, with a release of 1500 Gt carbon over periods varying from 500 to 20,000 years. They used the concentrations of methane and carbon dioxide to drive an atmospheric general circulation model (GCM) coupled to a mixed layer ocean model to study the impact of massive hydrate instability on Earth's climate. As expected, these model simulations of SS03 showed that a PETM-like case would cause dramatic climate change. Global temperatures increased by 6.7°C using a scenario with a release of 1.5 Gt carbon/year. Using a different experimental setup (i.e., an atmospheric GCM forced by SSTs based on PETM paleodata), *Huber and Sloan* [1999] simulated a considerably smaller global warming for the PETM (i.e., 2°C above the background early Eocene average paleotemperature). However, this difference in warming may be entirely due to the different experimental setup used by SS03 compared to the one used by *Huber and Sloan* [1999].

[6] An important drawback of the studies by SS03 and *Huber and Sloan* [1999] is that their models lack a representation of the three-dimensional ocean circulation. As a result, they were not able to simulate potential feedbacks of the oceanic circulation or to analyze long-term effects on the coupled atmosphere-ocean system. For instance, the impact on ocean temperature at different depths was not simulated. This is of special interest since the possibility exists that rapid warming caused by an initial methane release could trigger further hydrate instability through warming at intermediate water depths. Moreover, previous modeling studies could not investigate the response of the ocean thermohaline circulation (THC) to a massive methane release. Potentially, strong surface warming could lead to a decrease in deep sea ventilation at high latitudes due to a reduced surface water density, significantly weakening the THC and reducing the northward heat transport in the North Atlantic Ocean, thus providing a negative feedback here.

[7] To study these important phenomena, we have conducted two 2500-year-long transient experiments with a three-dimensional coupled atmosphere-sea ice-ocean model of intermediate complexity. Using the same 1.5 Gt/year scenario of SS03, we perturbed two different climate states: (1) a preindustrial climate state and (2) a much warmer climate state with a four times higher atmospheric CO_2 concentration than in the preindustrial climate state. These experiments enable us to address the following research questions that have not been considered before in modeling studies. What would be the response of the temperature distribution and circulation to a PETM-like emission scenario in a modern and "warm greenhouse" climate state? Do the intermediate waters warm up significantly, so that additional instabilities of methane hydrates might be triggered as suggested by *Bains et al.* [1999]? Is the strength of the THC reduced, resulting in a negative feedback in the North Atlantic Ocean? It is important to note that we do not intend to study the mechanism that causes the massive methane release or the impact of this release on the atmospheric methane and CO_2 concentrations, as our model setup is not suitable for this objective (i.e., no carbon cycle model included). Our simulations should be considered as sensitivity experiments to evaluate the ocean-atmosphere response in a "worst case" scenario of methane hydrate instability under preindustrial conditions and under enforced "warm greenhouse" conditions.

2. Model and Experimental Design

[8] We performed our experiments with the coupled atmosphere-sea ice-ocean model ECBilt-CLIO, version 3. The atmospheric component is ECBilt [*Opsteegh et al.*, 1998], a spectral quasi-geostrophic model with three vertical levels and a T21 horizontal resolution. It includes simple parameterizations for the diabatic heating due to radiative fluxes, the release of latent heat, and the exchange of sensible heat with the surface. ECBilt contains a full hydrological cycle that is closed over land by a simple model for soil moisture. Cloud cover is prescribed according to present-day climatology. The sea ice-ocean component, CLIO, consists of a free surface, primitive equation oceanic GCM with 20 vertical levels and $3° \times 3°$ latitude-longitude resolution, coupled to a comprehensive dynamic-thermodynamic sea-ice model [*Goosse and Fichefet*, 1999]. The only flux correction required in ECBilt-CLIO is an artificial reduction of precipitation over the Atlantic and Arctic Oceans, and a homogeneous distribution of this removed amount of freshwater over the Pacific Ocean [*Goosse et al.*, 2001].

[9] The version of ECBilt-CLIO used here is an updated and improved version of the model used earlier for a variety of applications, i.e., to simulate the modern climate [*Goosse et al.*, 2001, 2003], to study meltwater-induced abrupt climate events during the early Holocene [*Renssen et al.*, 2001, 2002], natural variability of the modern climate [*Goosse et al.*, 2002] and future climate evolution [*Goosse and Renssen*, 2001]. Compared to the earlier version, the present model simulates a climate that is closer to modern observations. The most important differences between the two model versions are a new land surface scheme that takes into account the heat capacity of the soil and the use of isopycnal diffusion as well as Gent and McWilliams pa-

Table 1. Summary of the Initial Conditions of the Two Emission Scenario Experiments[a]

Experiment	Duration, years	Initial Conditions	
		CO_2, ppmv	CH_4, ppbv
PREIND	1500	277	735
4*CO_2	1800	1110	735

[a]The Duration refers to the equilibrium simulation preceding the prescribed emission scenarios.

rameterization to represent the influence of mesoscale eddies in the ocean [*Gent and McWilliams*, 1990]. The climate sensitivity of ECBilt-CLIO is about 0.5°C/(W/m^2), which is at the lower end of the range (typically 0.5 to 1°C/(W/m^2)) found in most coupled climate models [*Cubasch et al.*, 2001].

[10] The initial conditions for our first experiment (hereinafter referred to as PREIND) were taken from a 1500-year-long simulation with constant forcings corresponding to the preindustrial climate (i.e., AD 1750, see Table 1). In addition, we performed a second experiment to study the impact of a methane pulse in a warm greenhouse climate. To obtain the initial conditions for this second experiment, we prescribed the same preindustrial forcings as in PREIND, except for the atmospheric CO_2 concentration, which was multiplied by four (hereinafter referred to as 4*CO_2, Table 1). This simulation reached a quasi-equilibrium after 1800 years. As a result of the higher atmospheric CO_2 concentration, the annual mean, globally averaged surface temperature is 3.1°C higher in 4*CO_2 compared to PREIND (i.e., 18.7°C versus 15.6°C, respectively) and the sea-ice area is much reduced. The annual mean area covered by sea ice in the Northern Hemisphere amounts to 12.4×10^6 km^2 and 9.2×10^6 km^2 in PREIND and 4*CO_2, respectively, whereas in the Southern Hemisphere the corresponding values are 14.0×10^6 km^2 and 3.3×10^6 km^2. In 4*CO_2, the ocean thermohaline circulation (THC) was slightly weaker, with 13.4 Sv (1 Sv = 10^6 m^3 s^{-1}) of North Atlantic Deep Water (NADW) exported at 20°S, compared to 14.6 Sv in PREIND.

[11] To study the effect of a massive methane release, we perturbed PREIND and 4*CO_2 by prescribing one of the PETM emission scenarios as discussed by SS03. In this particular scenario, the atmospheric methane concentration increases from a preindustrial concentration of 735 to 15600 ppbv within 100 years and remains at this level until year 1000 (Figure 1a). Subsequently, methane concentrations drop abruptly and remain at the preindustrial level for the rest of the experiment (i.e., until year 2500). According to the calculations of SS03, all the methane is oxidized into carbon dioxide, leading to an almost linear increase to a level about 1.5 times the initial concentration at the end of the methane release (i.e., from 277 to 435 ppmv in PREIND, and 1110 to 1267 ppmv in 4*CO_2, Figure 1b). After the methane concentration drops, the carbon dioxide concentration decreases, although it remains at a relatively high level (378 ppmv in PREIND; 1210 ppmv in 4*CO_2) during the remainder of the experiment due to the long atmospheric lifetime of carbon dioxide.

[12] According to SS03, this emission scenario represents a carbon release of about 1500 Gt. In the preindustrial case, this is in our model equivalent to a radiative forcing of 5.8 Wm^{-2} at the top of the troposphere. It is important to note that, in the 4*CO_2 case, the radiative forcing resulting from the scenario is less (i.e., 4.0 Wm^{-2}) due to a saturation effect that occurs at high CO_2 levels. The value of 4.0 Wm^{-2} is comparable to the radiative forcing due to a doubling of the modern atmospheric carbon dioxide content. In our experiments, we do not account for the increase in stratospheric water vapor discussed by SS03 since our model does not include a dynamic stratosphere. In the atmospheric GCM simulations of SS03, this feedback is also neglected. The rise in stratospheric water vapor concentration would be responsible for an additional radiative forcing of 1 Wm^{-2}.

3. Results

3.1. Surface Temperature

[13] The prescribed scenario produces a rapid warming in PREIND, with a 1.6°C increase in the global annual mean surface temperature from 15.6°C to 17.2°C in 250 years (Figure 2). Subsequently, the temperature rises by an additional 1°C in 750 years (from 17.2°C to 18.2°C), producing a total global surface warming of 2.6°C at the end of the period characterized by high methane levels (i.e., at year 1000). After 1000 years, cooling sets in due to the

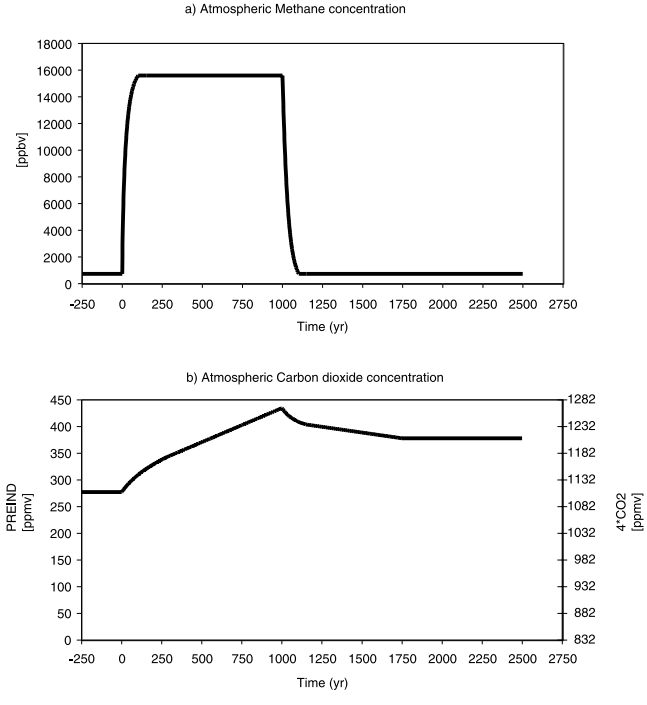

Figure 1. (a) Forcing time series of atmospheric concentrations of methane in ppbv and (b) carbon dioxide, in ppmv, based on calculations made by *Schmidt and Shindell* [2003]. Note that in Figure 1b the left axis is valid for PREIND, while the right axis is for 4*CO_2. The concentrations from year −250 to 0 represent the values for the reference climates, i.e., preindustrial: 735 ppbv for methane and 277 ppmv for carbon dioxide, and 4 times CO_2: 735 ppbv for methane and 1110 ppmv for carbon dioxide.

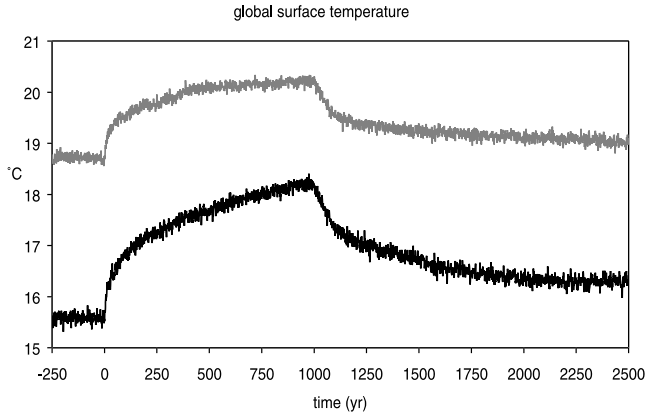

Figure 2. Simulated evolution of the annual mean global surface temperature (in °C) in PREIND (lower curve) and 4*CO_2 (upper curve).

fall in methane concentration, until a new equilibrium temperature of 16.3°C is reached at year 2000 that is governed by the 378 ppmv atmospheric carbon dioxide concentration. In 4*CO_2, the scenario results in a global surface temperature evolution that is similar in shape as in PREIND, but with a total warming limited to 1.5°C at year 1000 (i.e., 1.1°C less, Figure 2). This difference can be partly explained by the smaller radiative forcing in 4*CO_2 compared to PREIND.

[14] In both experiments, the temperature response is not equally distributed over all latitudes (Figures 3a–3b). At high latitudes, pronounced melting of snow and sea ice amplifies the warming involving two positive feedbacks. First, the well-known ice-albedo feedback, with reduced radiative heat loss when snow and sea ice melts, and second, the sea ice-insulation feedback, with an increasing heat flux from the ocean to the atmosphere when the insulating sea ice cover becomes thinner or even disappears. Locally, the annual mean surface temperature at peak warming is up to 10°C higher than in the reference climates, such as in the Weddell Sea where sea ice is no longer present. In contrast, the warming in the tropics is limited to 0.5° to 1°C.

3.2. Sea Ice

[15] The reduction in sea ice is stronger in the Southern Ocean than in the Arctic (Figures 4a–4b). In PREIND, the sea ice area averaged over the Northern Hemisphere is reduced by 22% (from 12.4 to 9.7 $\times$ 10^6 km^2), whereas in the Southern Hemisphere reduction is 64% (from 14.0 to 5.0 $\times$ 10^6 km^2). In 4*CO_2, the scenario causes a decrease in Arctic sea ice cover (25%, from 9.2 to 6.8 $\times$ 10^6 km^2) that is comparable to the decline in PREIND. Around Antarctica, hardly any sea ice in 4*CO_2 survives the warming due to the methane pulse, as only 0.7 $\times$ 10^6 km^2 in annual mean remains at year 400 compared to 3.3 $\times$ 10^6 km^2 at the start of the experiment, making the Southern Ocean almost ice-free. As a consequence, the positive feedbacks involving sea ice discussed earlier are considerably less powerful in 4*CO_2 than in PREIND, thus contributing to the difference in warming noted in Figures 2 and 3. In PREIND, the strong reduction in Southern Ocean sea ice cover also implies that some parts of the Antarctic coastal seas become practically ice-free throughout the year (i.e., on the western side of the Antarctic Peninsula between 90 and 110°W and between 30 and 60°E (not shown)). It should be noted that the decrease in sea ice cover in the Southern Ocean is slow compared to the Arctic. The strong and relatively slow response of the Southern Ocean sea ice can be explained by a two-phase mechanism described earlier by *Goosse and Renssen* [2001]. First, the warming is delayed because of the large heat capacity of the ocean and second, the warming is amplified through an enhanced meridional heat transport toward the Southern Ocean.

3.3. Ocean Circulation

[16] The global warming in the PREIND simulation causes a slight weakening of the THC, with 13.6 Sv of NADW transported at 20°S during peak warming compared to 14.6 Sv in the preindustrial control climate (Figure 5a). Moreover, the NADW cell becomes somewhat shallower at the expense of the AABW (Antarctic Bottom Water) cell (compare Figure 6c with Figure 6a). These changes in the

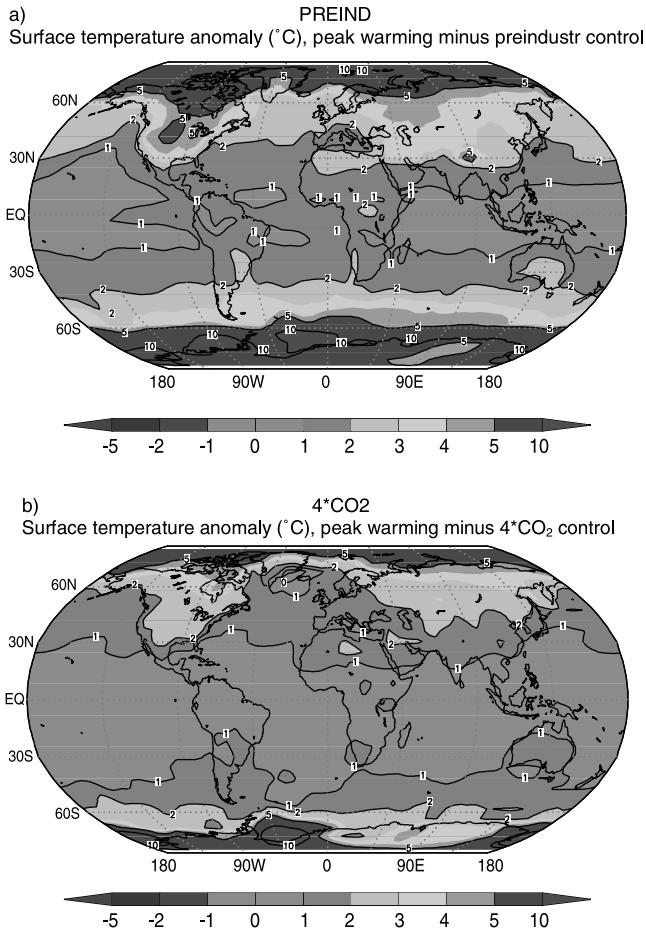

Figure 3. Simulated annual mean surface temperature anomaly (°C): peak warming (averaged over year 750 to 1000) minus the reference climate (year −250 to 0). Contours at 0.5, 1, 2, 3, 4, 5, and 10°C. See color version of this figure at back of this issue.

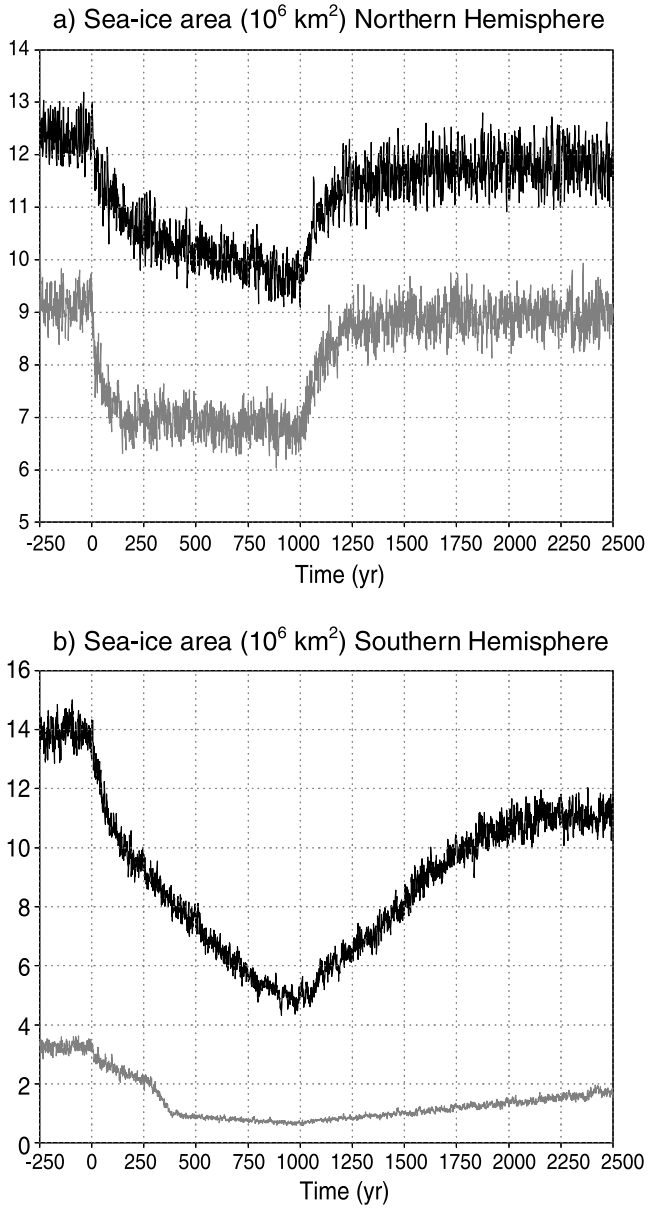

Figure 4. Simulated time series of the annual mean sea ice cover (in 10^6 km^2) in the (a) Northern and (b) Southern Hemispheres. Upper curves represent PREIND; lower curves represent 4*CO_2.

North Atlantic occur within the first 250 years of experiment PREIND (i.e., the period of strongest warming; Figures 5a and 6b). At the end of experiment PREIND, the THC state is very similar to the preindustrial state, although the NADW cell is still slightly weaker (Figure 6d). In experiment 4*CO_2, the THC weakening is hardly visible, with only a marginal reduction of NADW export between year 250 and 800 (Figure 5b).

[17] In the Southern Ocean, the export of circumpolar deep water strongly decreases in both experiments during the initial warming phase (first 250 years), namely from 17 to 12 Sv in PREIND (Figure 7a) and from 20 to 15 Sv in 4*CO_2 (Figure 7b). This reduction is most probably caused by the warming of the surface waters (by up to 5°C), stabilizing the water column and decreasing the deep mixing. The reduced circumpolar deep water export is consistent with the weakening of the overturning cell centered at 70°S (compare Figure 8b with Figure 8a). Subsequently, after year 250, the overturning cell strengthens again (Figure 8c), and the export of circumpolar deep water increases to 25 Sv in year 1150 (Figures 7a–7b). In PREIND, the strength of the Antarctic circumpolar current (ACC) follows the same pattern, as the mass transport through Drake Passage first declines in the initial 250 years from 127 to 122 Sv, and subsequently increases to 150 Sv in year 1100 (Figure 9). This evolution is linked to the development of the sea ice cover in PREIND, which is characterized by a slow reduction until year 1000 (Figure 4b). As parts of the Southern Ocean become ice-free, deep open ocean convection is increasing at several locations between year 500 and 1500. When cooling sets in after year 1000, the sea ice cover increases again and the ACC weakens, reaching values found in the preindustrial climate around year 2000. In the warmer climate in experiment 4*CO_2, the ACC is already strong from the start and shows a relatively small increase (Figure 9b), while deep open ocean convection is occurring in the Southern Ocean throughout the experiment.

[18] The export of AABW to the Atlantic Ocean, on the other hand, shows a deviant behavior. In PREIND, it increases in the first 250 years and becomes stronger than in the preindustrial reference climate (5.8 Sv), varying between 6.2 and 7.8 Sv (Figure 10a). This is related to the weakening and shallowing of the NADW overturning cell (Figures 6a–6d), giving AABW the opportunity to flow into the Atlantic basin. A similar, but weaker, response can be observed in experiment 4*CO_2 (Figure 10b).

3.4. Ocean Temperature

[19] The evolution of the global mean ocean temperature is more gradual than the surface temperature due to the thermal inertia of the oceans (Figure 11). In both PREIND and 4*CO_2, the total oceanic warming at year 1000 amounts to 1.1°C. This is surprising, as the radiative forcing represented by the scenario is less in 4*CO_2 than in PREIND (i.e., a 1.8 Wm^{-2} difference). We discussed earlier that the surface warming in 4*CO_2 is modest (Figure 2), implying that the deep ocean experiences relatively stronger warming compared to the upper ocean. This is confirmed by the latitude-depth profiles (Figures 12a–12d), which show in PREIND stronger warming in the upper ocean than in 4*CO_2, while the latter experiment shows more warming in the deeper ocean layers (mostly 0.5 to 1°C compared to generally less than 0.5°C in PREIND). The difference in the deep ocean response between the two experiments can be explained by the production of relatively warm AABW in the Southern Ocean in experiment 4*CO_2. Indeed, a strong warm anomaly is noticed at depth south of 60°S in Figure 12b.

[20] In both experiments, the strongest warming occurs in the mixed layer in the Southern Ocean, with a 4°C increase at ~60 to 70°S. At high northern latitudes, the warming is less, with temperatures being between 2 to 3°C higher in the

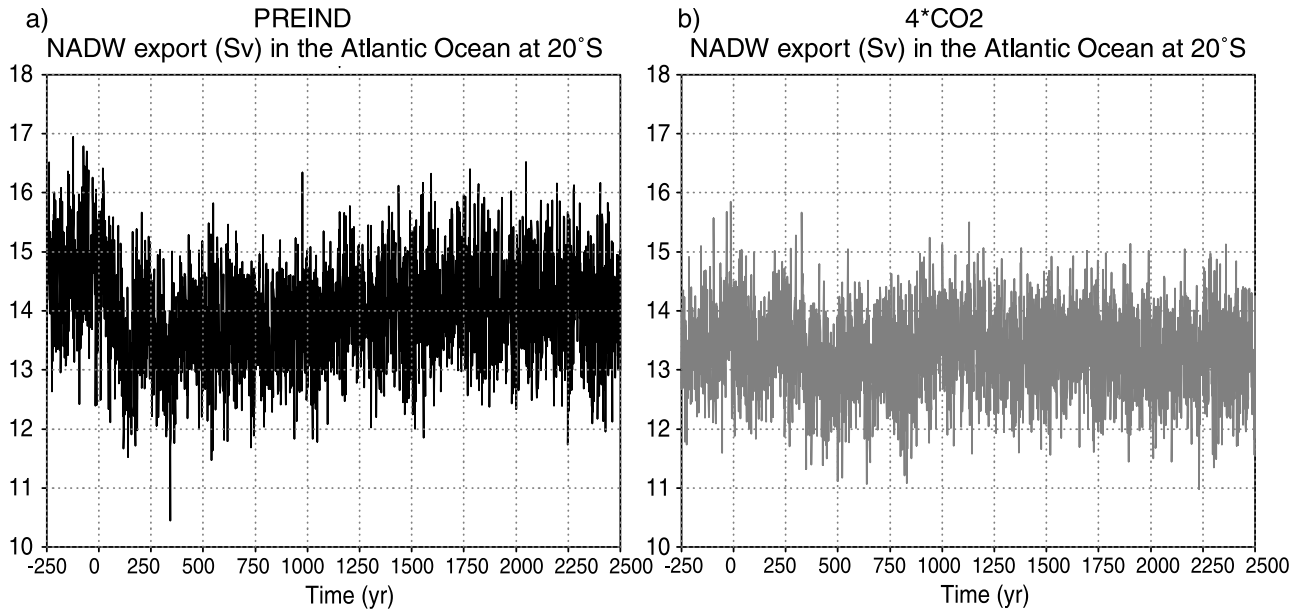

Figure 5. Simulated time series of annual mean values of NADW export (Sv) in the Atlantic Ocean at 20°S: (a) PREIND; (b) 4*CO_2. The first 250 years (t = −250 to 0) represent the reference climate equilibrium.

upper 100 m than in the preindustrial climate in PREIND. At low latitudes, the temperature increase in the mixed layer is restricted to 0.5 to 1.5°C, but the changes are larger at intermediate depths (100–1000 m). At those depths, the waters are relatively warm at all latitudes, with temperatures being mostly 1 to 3°C or higher than in the reference climates. In PREIND, this warming at intermediate depths is most pronounced in the Atlantic basin (Figure 12c), and can locally be up to 4 to 5°C (not shown). The maximum temperature increase at intermediate depth appears to have its origin at surface in the region of intermediate water formation at 50 to 60° latitude in both hemispheres. The intermediate waters in the Atlantic also become more saline (between 0.1 and 0.4 psu, not shown), suggesting that downwelling of relatively warm and saline surface waters takes place there.

4. Discussion

[21] In our experiments, we have perturbed two different climates (a preindustrial state and a warm "greenhouse" state) by prescribing a drastic scenario of massive methane release. We have deliberately taken a "worst case" emission scenario based on the PETM as this enables studying the upper bounds of the climate response to widespread methane hydrate instability. Indeed, as expected from paleodata, we found that this scenario leads to significant climate change in the model, including strong global warming (up to 2.6°C) and important changes in the ocean overturning circulation. If this scenario would become reality in the future (i.e., instability of methane hydrates at the PETM scale due to anthropogenic warming), these changes could take place in addition to climate changes caused by anthropogenic forcing. When considering this possibility, however, it is good to realize that many uncertainties are involved in model experiments like the ones described here.

[22] First, several feedbacks have not been accounted for in the chemical model study by SS03, implying that the used scenario is most probably incomplete. These feedbacks include the effects of changes in temperature and humidity on atmospheric reaction rates, the impact of productivity changes on the uptake of carbon, and the interactions between the troposphere and stratosphere [*Schmidt and Shindell*, 2003]. Moreover, the applied scenario assumes that the methane was released quite rapidly (i.e., 1500 Gt within 1000 years, following [e.g., *Norris and Röhl*, 1999; *Röhl et al.*, 2000]), but this may not be realistic, as there is still considerable debate on the characteristics of the methane release during the PETM [e.g., *Bains et al.*, 2000].

[23] Second, we have neglected several potentially important processes due to simplifications in ECBilt-CLIO. For instance, the cloud cover was not allowed to change as measured values are prescribed, and the effect of changes in stratospheric water vapor content was not included as a dynamical stratosphere is lacking in our model. According to previous modeling studies [*Sloan and Pollard*, 1998; *Peters and Sloan*, 2000], high methane levels could induce an increase in polar stratospheric clouds, which would enhance the warming. On the other hand, low level cloud cover tends to increase when the sea ice cover decreases, thus causing an increase in the cloud albedo that could partially compensate for the effect of a reduced ice cover on the radiation balance [e.g., *Ebert and Curry*, 1993]. We have not been able to take these effects into account, as simplifications are inevitable given the long timescale involved in this study. In addition, as no carbon cycle module is included in our model, we had to prescribe the atmospheric

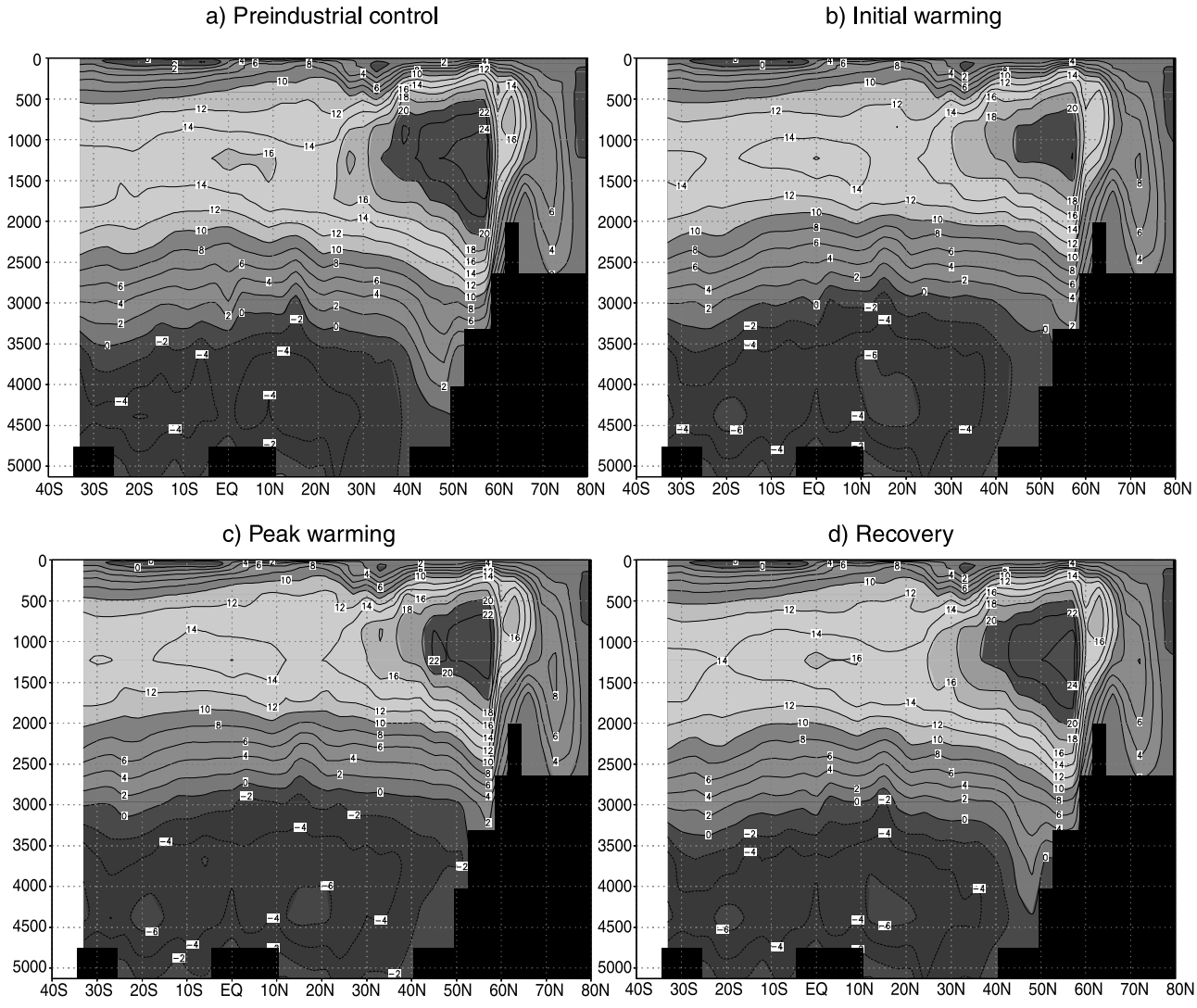

Figure 6. Latitude-depth distributions of the annual mean meridional overturning stream function in the Atlantic Ocean for four different phases of the experiment: (a) preindustrial control, (b) initial warming (year 250), (c) peak warming (year 1000), and (d) recovery phase (year 2500). Contour interval is 2 Sv. Flow is clockwise along positive contours. See color version of this figure at back of this issue.

trace gas concentrations, so that the simulated warming had no effect on the content of methane and carbon dioxide in the atmosphere, for instance due to further methane hydrate instability.

[24] Some idea of the physical consistency of our experiments can be obtained by comparing the simulation results with paleoevidence from the PETM. The latest Paleocene climate prior to the PETM was considerably warmer than the preindustrial climate (i.e., a few degrees centigrade), with a smaller surface covered by snow and ice [e.g., *Huber and Sloan*, 1999]. Consequently, the conditions in our $4*CO_2$ experiment are more appropriate for modeling the PETM than those of PREIND. However, the continental configuration during the early Paleogene was different, including an open Panama Strait and a much narrower Drake Passage [e.g., *Zachos et al.*, 1993]. Nevertheless, a model study by *Huber and Sloan* [2001] suggests that, despite these different conditions, the global ocean circulation in the early Eocene was not dissimilar to the modern state, with NADW formed in the North Atlantic, and near-modern ocean heat transport and temperature gradients.

[25] Forced by a PETM-like emission scenario, our model simulates oceanic surface warming varying from 8 to 5°C at high latitudes, to 2 to 4°C in the subtropics, to less than 1 to 2°C in tropical oceans. These model results are similar to the PETM surface warming indicated by the sparse marine data available. In the Weddell Sea at high southern latitudes (ODP 690 at 69°S), reconstructions suggest a SST increase of 4 to 8°C over the PETM [*Kennett and Stott*, 1991; *Thomas et al.*, 2002]. In addition, in the subtropical Atlantic (Walvis Ridge, DSDP 527 at 35°S), the estimated SST increase is 1 to 4°C [*Thomas et al.*, 1999]. Two low latitude records (ODP 1001, tropical Atlantic at 10°N, ODP 865, tropical Pacific) suggest that the SST rise in the tropics was

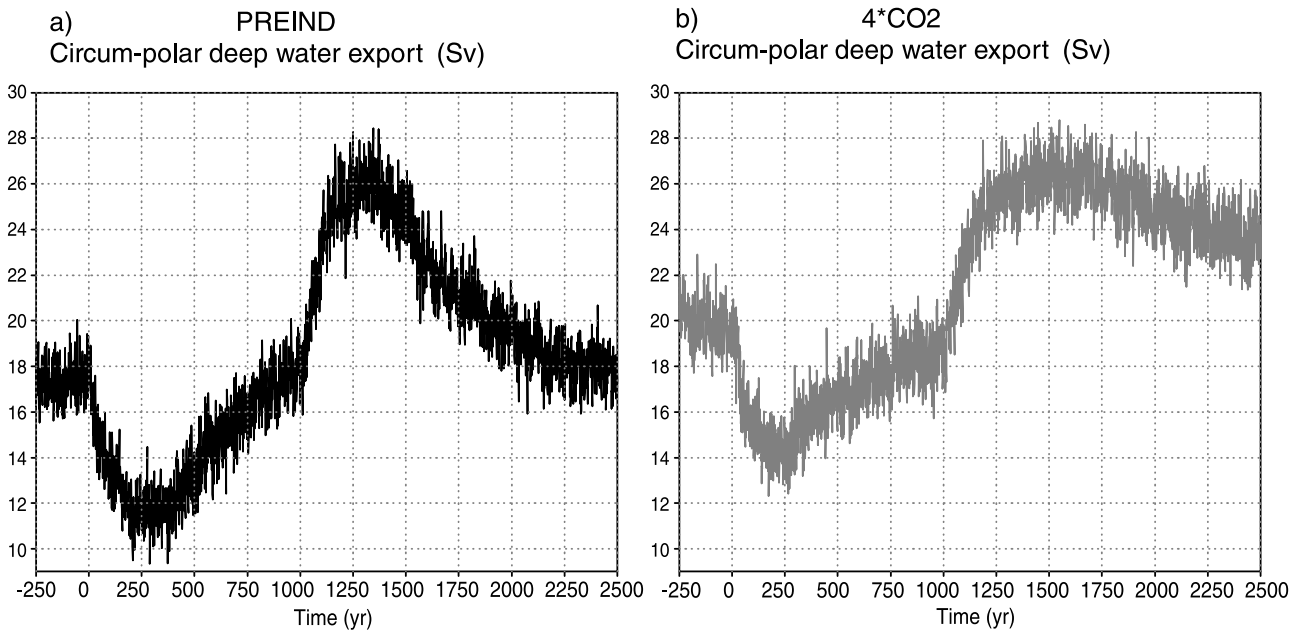

Figure 7. Simulated time series of annual mean values of total export of total circum-polar deep water (Sv): (a) PREIND; (b) 4*CO_2. The first 250 years (t = −250 to 0) represent the reference climate equilibrium.

minor (about 1°C [*Bralower et al.*, 1995, 1997]), although a recent SST estimate for the tropical Pacific based on Mg/Ca ratios indicates a considerably stronger warming (4 to 5°C [*Zachos et al.*, 2003]). Generally, model and data are consistent for the surface ocean and both indicate a high-latitude temperature amplification due to the massive methane release. A temperature reconstruction by *Fricke et al.* [1998] for a terrestrial site in Wyoming (∼43°N) fits in this pattern, as here the increase during the PETM is estimated at 2 to 4°C, which is similar in our results. Moreover, our estimate of a global surface temperature increase of 1.5°C (in 4*CO_2) due to the massive methane release is close to the 2°C found in the model study on the PETM by *Huber and Sloan* [1999]. Calculations by SS03, however, show a much stronger global warming of 6.7°C for the same PETM scenario (1.5 Gt carbon per year) we have prescribed in our experiments. Using a less extreme scenario (0.3 Gt/year), they simulated a global temperature increase of 2.9°C. Most probably, the difference between our result and the model study of SS03 can be explained by variations in the sensitivity to radiative forcing, as this sensitivity is known to differ considerably (i.e., by a factor 2) between models [*Cubasch et al.*, 2001].

[26] Our simulation indicates less warm conditions for the deep ocean than suggested by proxy data for the PETM. Temperature reconstructions for 1500–2000 m water depths suggest an increase of about 5°C for the Weddell Sea, the tropical Pacific, and the subtropical Atlantic (Blake Nose, ODP 1051, 35°N) [*Bralower et al.*, 1995; *Katz et al.*, 1999; *Thomas et al.*, 2002], while in our experiment the temperature increase at this depth is up to 1 to 2.5°C. The relatively high temperatures shown by paleodata at 1500–2000 m water depths could indicate that during the PETM the THC was significantly weakened or even shut-down, as several model studies have shown that this would lead to warmer deep waters (by a few degrees centigrade [e.g., *Manabe and Stouffer*, 1988]). In our simulation, no collapse of the THC occurs, it only becomes somewhat weaker and shallower, similar to what is found in most coupled model simulations with anthropogenic forcing for the 21st century [*Cubasch et al.*, 2001]. In the latter experiments, a similar radiative forcing (∼6 W/m^2) is prescribed as in our experiment. It should be realized, however, that model experiments by *Huber and Sloan* [2001] suggest that the THC was much weaker in the latest Paleocene than in the modern state. Ocean model studies indicate that a weak THC is generally closer to the threshold instability point, implying that it is conceivable that the climate of the latest Paleocene/early Eocene was more sensitive to perturbations leading to a further reduction in THC. Thus the difference between our results for the deep ocean and the PETM paleoevidence might be explained by the difference between the reference states (i.e., preindustrial or 4*CO_2 and latest Paleocene). It should also be noted that most estimates of paleotemperatures are based on oxygen isotopes, which could also have been influenced by salinity, thus implying that the temperature reconstructions have a considerable uncertainty range.

[27] Our results have shed some light on the effect of a PETM emission scenario on the ocean circulation and temperature distribution. Unfortunately, the design of our experiments (i.e., using a model without a carbon cycle module) does not permit addressing the issue of the mechanism behind the PETM in detail. For instance, we are unable to see if the catastrophic methane release was solely responsible for the total warming observed during the PETM, or if perhaps the methane pulse was merely trig-

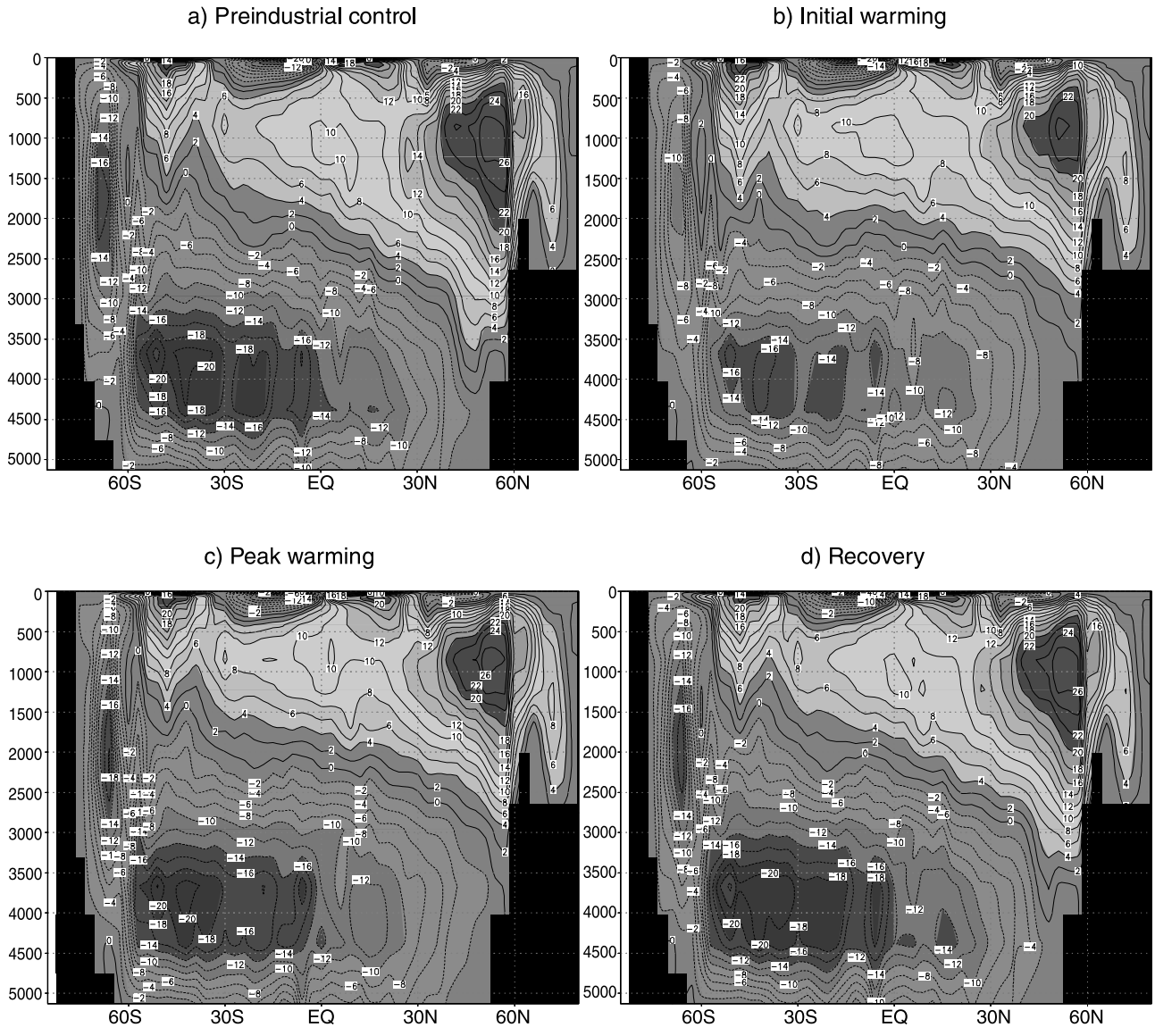

Figure 8. Latitude-depth distributions of the annual mean meridional overturning stream function in the global ocean for four different phases of the experiment: (a) preindustrial control, (b) initial warming (year 250), (c) peak warming (year 1000), and (d) recovery phase (year 2500). Contour interval is 2 Sv. Flow is clockwise along positive contours. See color version of this figure at back of this issue.

gered by warming forced by another process. However, we can speculate that the 1 to 3°C warming of intermediate waters simulated in our experiments could lower the upper limit of the hydrate stability zone, thus potentially causing further thermal dissociation of methane hydrates. If this warming would occur today, the stability diagram presented by *Dickens et al.* [1995, Figure 1] suggests that the lowering of the upper limit of the hydrate stability zone would be modest (i.e., in the order of 50 m, from 250 to 300 m water depth), although it should be noted that the stability zone of methane hydrates increases exponentially over this depth interval [*Nisbet*, 1992]. This implies that additional releases could occur. The amount of methane involved would be in the order of a few percent of the present-day oceanic methane hydrate reservoir [*Dickens et al.*, 1995], which would result in a minor positive feedback. However, it should be noted that considerable amounts of methane hydrates are stored at a relatively shallow depth (~200 m) at high latitudes [e.g., *Buffet*, 2000]. In our model the strongest warming occurs at high latitudes, where locally the temperature increase at 200 m is 5 to 8°C. This suggests that possibly the additional methane releases could be more extensive, resulting in a stronger positive feedback. Future experiments with more sophisticated models are required to study these effects.

5. Conclusions

[28] We have conducted two 2500-year-long experiments with a 3-D, global coupled atmosphere-sea ice-ocean model

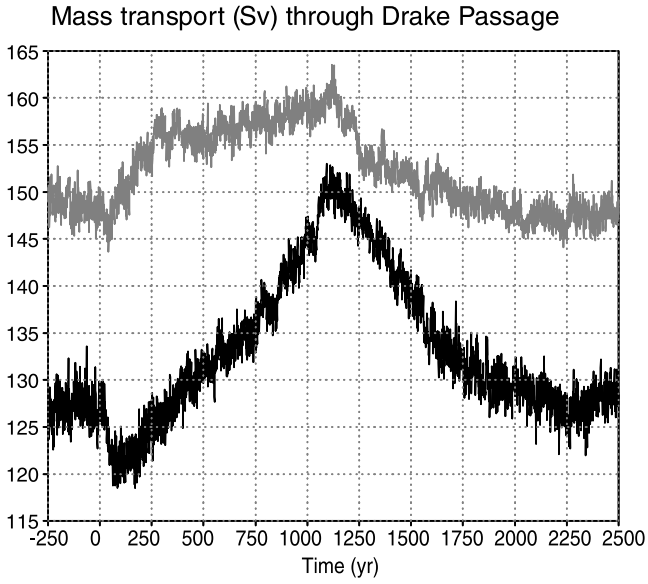

Figure 9. Simulated time series of annual mean values of the strength of the ACC: mass transport through Drake Passage (Sv). Lower curve: PREIND; upper curve: 4*CO_2. The first 250 years (t = −250 to 0) represent the reference climate equilibrium.

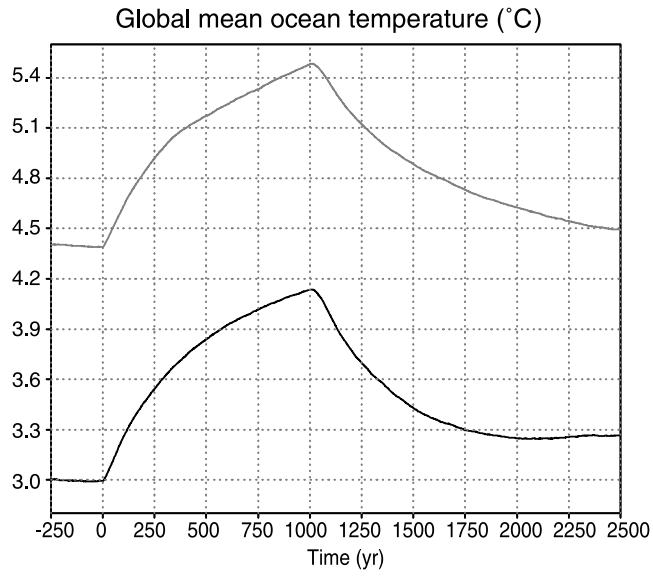

Figure 11. Simulated evolution of the annual mean global ocean temperature (°C). Lower curve represents PREIND; upper curve represents 4*CO_2.

of intermediate complexity in which 1500 Gt of methane carbon were added to the atmosphere. The two simulations differed in their initial climate states: (1) a climate in equilibrium with preindustrial forcing conditions, and (2) as (1) but with a 4 times elevated atmospheric CO_2 concentration. Our objective was to study the response of the temperature distribution and circulation to a massive methane release (for which we have taken a PETM-like emission scenario) in a modern and "warm greenhouse" climate state, thereby focusing on the impact on the oceanic temperature at different depths and on the ocean circulation. The applied scenario is equivalent to a radiative forcing at the top of the troposphere of 5.8 Wm^{-2} in the preindustrial case and 4.0 Wm^{-2} in the 4*CO_2 case. The experimental results suggest the following response of the coupled atmosphere-ocean system.

[29] 1. The simulated response in the surface temperature reveals large differences between latitudinal zones. At high latitudes, the warming is amplified due to two positive feedbacks (i.e., the ice-albedo feedback and the

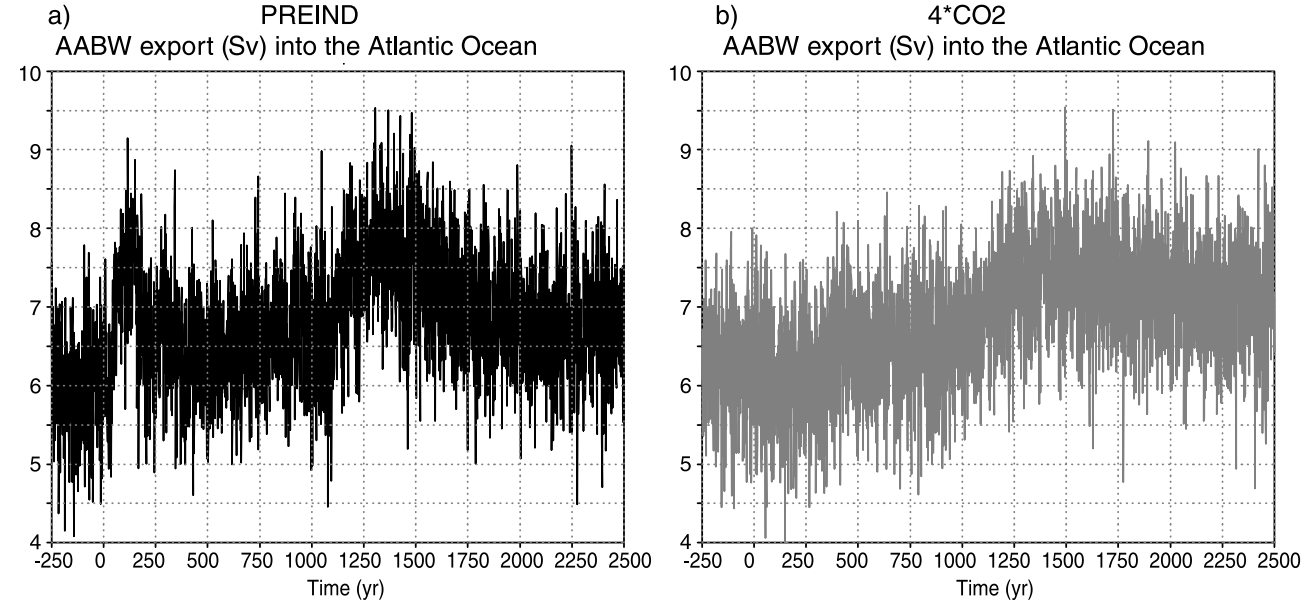

Figure 10. Simulated time series of annual mean values of AABW export (Sv) into the Atlantic Ocean: (a) PREIND; (b) 4*CO_2. The first 250 years (t = −250 to 0) represents the preindustrial equilibrium.

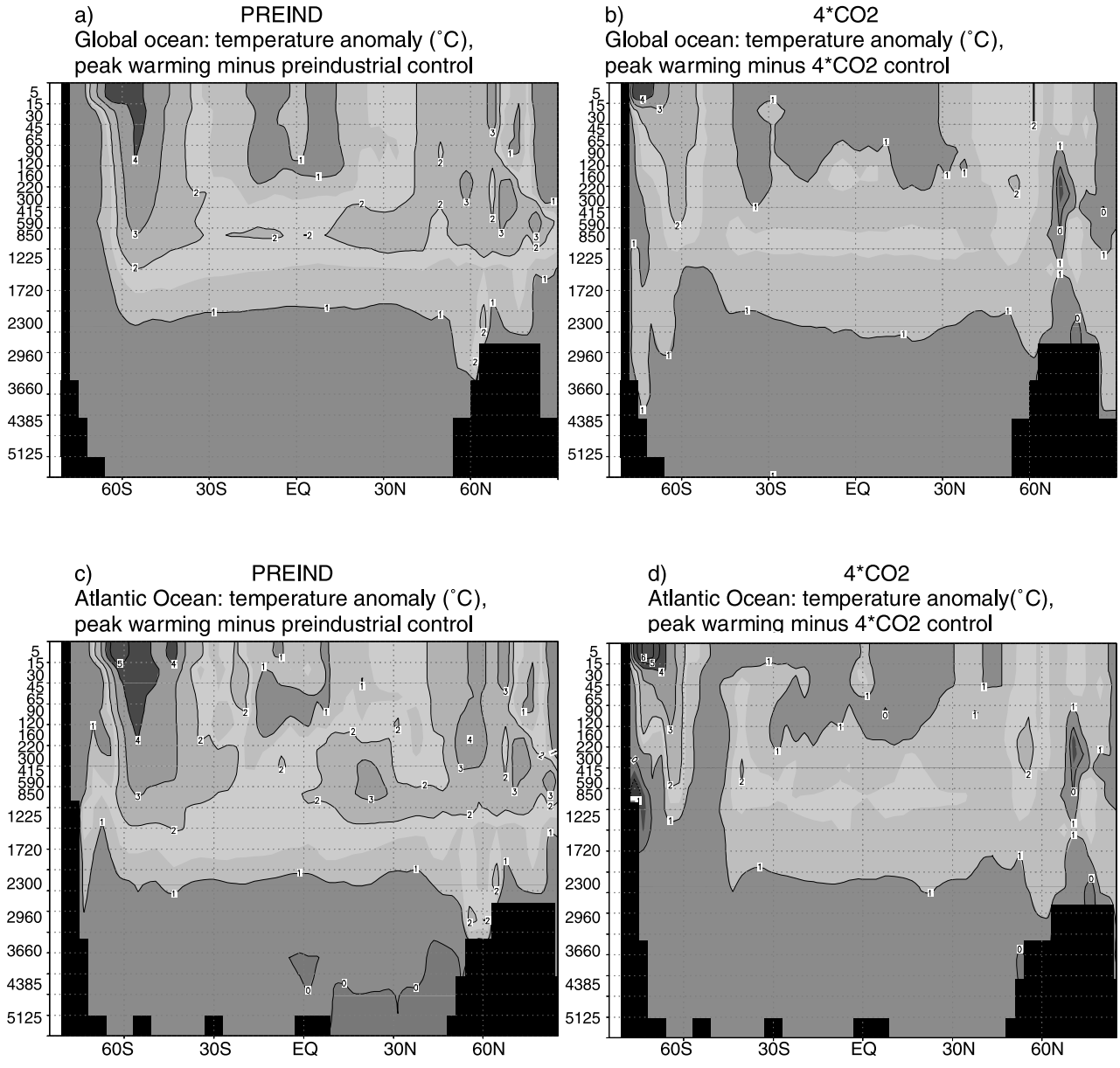

Figure 12. Latitude-depth distribution of the ocean temperature anomaly (°C): peak warming (year 1000) minus reference climate: (a) global ocean PREIND, (b) global ocean 4*CO_2, (c) Atlantic Ocean PREIND, and (d) Atlantic Ocean 4*CO_2. See color version of this figure at back of this issue.

sea ice-insulation feedback), resulting in a surface temperature rise of up to 10°C, whereas at low latitudes the surface temperature increase was about 1°C. The global mean surface warming in the case of preindustrial forcings is 2.6°C in 1000 years, of which 1.6°C occurred in the first 250 years. In the 4*CO_2 case, the total warming was 1.5°C in 1000 years. This difference can be explained by a combination of the small radiative forcing in the 4*CO_2 case and the reduced efficiency of the two positive feedbacks involving sea ice in a warmer climate. The simulated results for the surface ocean are consistent with proxy evidence for the PETM event.

[30] 2. In the warm 4*CO_2 climate, the warming of the deep ocean due to a massive methane release is more efficient (+0.5 to +1°C) than in the preindustrical case (mostly less than +0.5°C) in consequence of the formation of relatively warm AABW. The simulated temperature of intermediate waters (100 to 1000 m) rises by 1 to 3°C, especially in the Atlantic basin in the preindustrial case. This could lead to a lowering of the upper limit of the hydrate stability zone, which could result in additional releases of methane (estimated at 1–2% of the modern oceanic methane hydrate reservoir). This would result in an additional positive feedback.

[31] 3. No major reorganization of the THC is found in the model. The NADW overturning cell of the THC becomes slightly shallower and weaker (1 Sv export at 20°S in the preindustrial case), whereas the AABW overturning cell

strengthens and expands. In the deep ocean, the model results show a smaller warming (1 to 2.5°C) than suggested by PETM paleodata (~5°C). This difference could be related to the strength of the THC. Previous experiments suggest that, compared to our reference states, the THC was much weaker during the latest Paleocene and possibly more sensitive to perturbations. Consequently, the relatively warm deep ocean indicated by PETM paleodata could result from a further reduction in THC during the PETM.

[32] 4. In the Southern Ocean deep open ocean convection becomes possible in both experiments and the sea ice cover is considerably reduced, which is accompanied by an intensification of the ACC.

[33] **Acknowledgments.** The constructive comments of G. R. Dickens and G. A. Schmidt are gratefully acknowledged. T. Fichefet and H. Goosse are research associates at the National Fund for Scientific Research (Belgium). H. Renssen is supported by the Netherlands Organization for Scientific Research.

References

Bains, S., R. M. Corfield, and R. D. Norris (1999), Mechanisms of climate warming at the end of the Paleocene, *Science*, *285*, 724–727.

Bains, S., R. D. Norris, R. M. Corfield, and K. L. Faul (2000), Termination of global warmth at the Palaeocene/Eocene boundary through productivity feedback, *Nature*, *407*, 171–174.

Bice, K. L., and J. Marotzke (2001), Numerical evidence against reversed thermohaline circulation in the warm Paleocene/Eocene ocean, *J. Geophys. Res.*, *106*, 11,529–11,542.

Bice, K. L., and J. Marotzke (2002), Could changing ocean circulation have destabilized methane hydrate at the Paleocene/Eocene boundary?, *Paleoceanography*, *17*(2), 1018, doi:10.1029/2001PA000678.

Bralower, T. J., J. C. Zachos, E. Thomas, M. Parrow, K. Paull, D. C. Kelly, I. P. Silva, W. V. Sliter, and K. C. Lohmann (1995), Late Paleocene to Eocene paleoceanography of the equatorial Pacific Ocean: Stable isotopes recorded at Ocean Drilling Program Site 865, Allison Guyot, *Paeoceanography*, *10*, 841–865.

Bralower, T., D. J. Thomas, J. C. Zachos, M. M. Hirschmann, U. Röhl, H. Sigurdsson, E. Thomas, and D. L. Whitney (1997), High-resolution records of late Paleocene thermal maximum and circum-Caribbean volcanism: Is there a causal link?, *Geology*, *25*, 963–966.

Brooks, E. J., S. Harder, J. Severinghaus, E. J. Steig, and C. M. Sucher (2000), On the origin and timing of rapid changes in atmospheric methane during the last glacial period, *Global Biogeochem. Cycles*, *14*, 559–572.

Buffet, B. A. (2000), Clathrate hydrates, *Annu. Rev. Earth Planet. Sci.*, *28*, 477–507.

Cubasch, U., G. A. Meehl, G. J. Boer, R. J. Stouffer, M. Dix, A. Noda, C. A. Senior, S. Raper, and K. S. Yap (2001), Projections of future climate change, in *Climate Change 2001: The Scientific Basis, Contributions of Working Group I to the Third Assessment Report of the IPCC*, edited by J. T. Houghton et al., pp. 525–582, Cambridge Univ. Press, New York.

Dickens, G. R. (2000), Methane oxidation during the late Palaeocene thermal maximum, *Bull. Soc. Geol. Fr.*, *171*, 37–49.

Dickens, G. R. (2001), The potential volume of oceanic methane hydrates with variable external conditions, *Org. Geochem.*, *32*, 1179–1193.

Dickens, G. R. (2003), A methane trigger for rapid warming?, *Science*, *299*, 1017.

Dickens, G. R., J. R. O'Neil, D. K. Rea, and R. M. Owen (1995), Dissociation of oceanic methane hydrate as a cause of the carbon isotope excursion at the end of the Paleocene, *Paleoceanography*, *10*, 965–971.

Dickens, G. R., M. M. Castillo, and J. C. G. Walker (1997), A blast of gas in the latest Paleocene: Simulating first-order effects of massive dissociation of oceanic methane hydrate, *Geology*, *25*, 259–262.

Ebert, E. E., and J. A. Curry (1993), An intermediate one-dimensional thermodynamic sea ice model for investigating ice-atmosphere interactions, *J. Geophys. Res.*, *98*(C6), 10,085–10,109.

Fricke, H. C., W. C. Clyde, J. R. O'Neil, and P. D. Gingerich (1998), Evidence for rapid climate change in North America during the latest Paleocene thermal maximum: Oxygen isotope compositions of biogenic phosphate from Bighorn Basin (Wyoming), *Earth Planet. Sci. Lett.*, *160*, 193–208.

Gent, P. R., and J. C. McWilliams (1990), Isopycnal mixing in ocean general circulation models, *J. Phys. Oceanogr.*, *20*, 150–155.

Goosse, H., and T. Fichefet (1999), Importance of ice-ocean interactions for the global ocean circulation: A model study, *J. Geophys. Res.*, *104*, 23,337–23,355.

Goosse, H., and H. Renssen (2001), A two-phase response of Southern Ocean to an increase in greenhouse gas concentrations, *Geophys. Res. Lett.*, *28*, 3469–3473.

Goosse, H., F. M. Selten, R. J. Haarsma, and J. D. Opsteegh (2001), Decadal variability in high northern latitudes as simulated by an intermediate complexity climate model, *Ann. Glaciol.*, *33*, 525–532.

Goosse, H., H. Renssen, F. M. Selten, R. J. Haarsma, and J. D. Opsteegh (2002), Potential causes of abrupt climate events: A numerical study with a three-dimensional climate model, *Geophys. Res. Lett.*, *29*(18), 1860, doi:10.1029/2002GL014993.

Goosse, H., F. M. Selten, R. J. Haarsma, and J. D. Opsteegh (2003), Large sea-ice volume anomalies simulated in a coupled climate model, *Clim. Dyn.*, *20*, 523–536.

Harvey, L. D. D., and H. Zhen (1995), Evaluation of the potential impact of methane clathrate destabilization on future global warming, *J. Geophys. Res.*, *100*, 2905–2926.

Hinrichs, K. U., L. R. Hmelo, and S. P. Sylva (2003), Molecular fossil record of elevated methane levels in late Pleistocene coastal waters, *Science*, *299*, 1214–1217.

Huber, M., and L. C. Sloan (1999), Warm climate transitions: A general circulation modeling study of the Late Paleocene Thermal Maximum (LPTM), *J. Geophys. Res.*, *104*, 16,633–16,655.

Huber, M., and L. C. Sloan (2001), Heat transport, deep waters, and thermal gradients: Coupled simulation of an Eocene greenhouse climate, *Geophys. Res. Lett.*, *28*, 3481–3484.

Katz, M. E., D. K. Pak, G. R. Dickens, and K. G. Miller (1999), The source and fate of massive carbon input during the latest Paleocene thermal maximum, *Science*, *286*, 1531–1533.

Kennett, J. P., and L. D. Stott (1991), Abrupt deep-sea warming, palaeoceanographic changes and benthic extinctions at the end of the Paleocene, *Nature*, *353*, 225–229.

Kennett, J. P., K. G. Cannariato, I. L. Hendy, and R. J. Behl (2000), Carbon isotope evidence for methane hydrate instability during Quaternary interstadials, *Science*, *288*, 128–133.

Kennett, J. P., K. G. Cannariato, I. L. Hendy, and R. J. Behl (2002), *Methane Hydrates in Quaternary Climate Change: The Clathrate Gun Hypothesis*, *Spec. Publ.*, vol. 54, 224 pp., AGU, Washington, D. C.

Kvenvolden, K. A. (1988), Methane hydrate—A major reservoir of carbon in the shallow geosphere?, *Chem. Geol.*, *71*, 41–51.

Manabe, S., and R. J. Stouffer (1988), Two stable equilibria of a coupled ocean-atmosphere model, *J. Clim.*, *1*, 841–866.

Nisbet, E. G. (1990), Climate change and methane, *Nature*, *347*, 23.

Nisbet, E. G. (1992), Sources of atmospheric CH4 in early postglacial time, *J. Geophys. Res.*, *97*, 12,859–12,867.

Nisbet, E. G., and D. J. W. Piper (1998), Giant submarine landslides, *Nature*, *392*, 329–330.

Norris, R. D., and U. Röhl (1999), Carbon cycling and chronology of climate warming during the Palaeocene/Eocene transition, *Nature*, *401*, 775–778.

Opsteegh, J. D., R. J. Haarsma, F. M. Selten, and A. Kattenberg (1998), ECBILT: A dynamic alternative to mixed boundary conditions in ocean models, *Tellus, Ser. A*, *50*, 348–367.

Peters, R. B., and L. C. Sloan (2000), High concentrations of greenhouse gases and polar stratospheric clouds: A possible solution to high-latitude faunal migration at the latest Paleocene thermal maximum, *Geology*, *28*, 979–982.

Prather, M., et al. (2001), Atmospheric chemistry and greenhouse gases, in *Climate Change 2001: The Scientific Basis, Contributions of Working Group I to the Third Assessment Report of the IPCC*, edited by J. T. Houghton et al., pp. 239–287, Cambridge Univ. Press, New York.

Prentice, I. C., G. D. Farquhar, M. J. R. Fasham, M. L. Goulden, M. Heimann, V. J. Jaramillo, H. S. Kheshgi, C. Le Quéré, R. J. Scholes, and D. W. R. Wallace (2001), The carbon cycle and atmospheric carbon dioxide, in *Climate Change 2001: The Scientific Basis, Contributions of Working Group I to the Third Assessment Report of the IPCC*, edited by J. T. Houghton et al., pp. 183–237, Cambridge Univ. Press, New York.

Renssen, H., H. Goosse, T. Fichefet, and J. M. Campin (2001), The 8.2 kyr BP event simulated by a global atmosphere-sea-ice-ocean model, *Geophys. Res. Lett.*, *28*, 1567–1570.

Renssen, H., H. Goosse, and T. Fichefet (2002), Modeling the effect of freshwater pulses on the early Holocene climate: The influence of high-

frequency climate variability, *Paleoceanography*, *17*(2), 1020, doi:10.1029/2001PA000649.
Röhl, U., T. J. Bralower, R. D. Norris, and G. Wefer (2000), New chronology for the late Paleocene thermal maximum and its environmental implications, *Geology*, *28*, 927–930.
Rothwell, R. G., J. Thomson, and G. Kähler (1998), Low-sea-level emplacement of a very large Late Pleistocene "megaturbidite" in the western Mediterranean Sea, *Nature*, *392*, 377–380.
Schmidt, G. A., and D. T. Shindell (2003), Atmospheric composition, radiative forcing, and climate change as a consequence of a massive methane release from gas hydrates, *Paleoceanography*, *18*(1), 1004, doi:10.1029/2002PA000757.
Shellito, C. J., L. C. Sloan, and M. Huber (2003), Climate model sensitivity to atmospheric CO_2 levels in the early-middle Paleogene, *Palaeogeogr. Palaeoclimatol. Palaeoecol.*, *193*, 113–123.
Sloan, L. C., and D. Pollard (1998), Polar stratospheric clouds: A high latitude warming mechanism in an ancient greenhouse world, *Geophys. Res. Lett.*, *25*, 3517–3520.
Thomas, D. J., T. J. Bralower, and J. C. Zachos (1999), New evidence for subtropical warming during the late Paleocene thermal maximum: Stable isotopes from deep sea drilling project site 527, Walvis Ridge, *Paleoceanography*, *14*, 561–570.
Thomas, D. J., J. C. Zachos, T. J. Bralower, E. Thomas, and S. Bohaty (2002), Warming the fuel for the fire: Evidence for the thermal dissociation of methane hydrate during the Paleocene-Eocene thermal maximum, *Geology*, *30*, 1067–1070.
Zachos, J. C., K. C. Lohmann, J. C. G. Walker, and S. W. Wise (1993), Abrupt climate change and transient climates during the Paleogene: A marine perspective, *J. Geol.*, *101*, 191–213.
Zachos, J. C., M. W. Wara, S. Bohaty, M. L. Delaney, M. R. Petrizzo, A. Brill, T. J. Bralower, and I. Premoli-Silva (2003), A transient rise in tropical sea surface temperature during the Paleocene-Eocene Thermal Maximum, *Science*, *302*, 1551–1554.

C. J. Beets, D. Kroon, and H. Renssen, Faculty of Earth and Life Sciences, Vrije Universiteit Amsterdam, De Boelelaan 1085, Amsterdam, NL-1081HV, Netherlands. (hans.renssen@geo.falw.vu.nl)

T. Fichefet and H. Goosse, Institut d'Astronomie et de Géophysique Georges Lemaître, Université Catholique de Louvain, 2 Chemin du Cyclotron B-1348, Louvain-la-Neuve, Belgium.

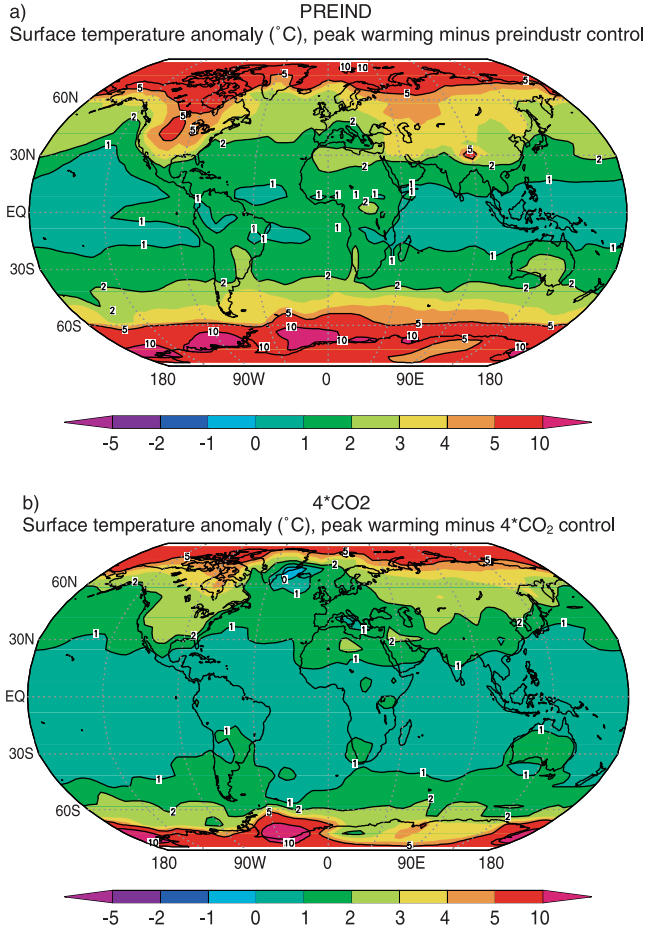

Figure 3. Simulated annual mean surface temperature anomaly (°C): peak warming (averaged over year 750 to 1000) minus the reference climate (year −250 to 0). Contours at 0.5, 1, 2, 3, 4, 5, and 10°C.

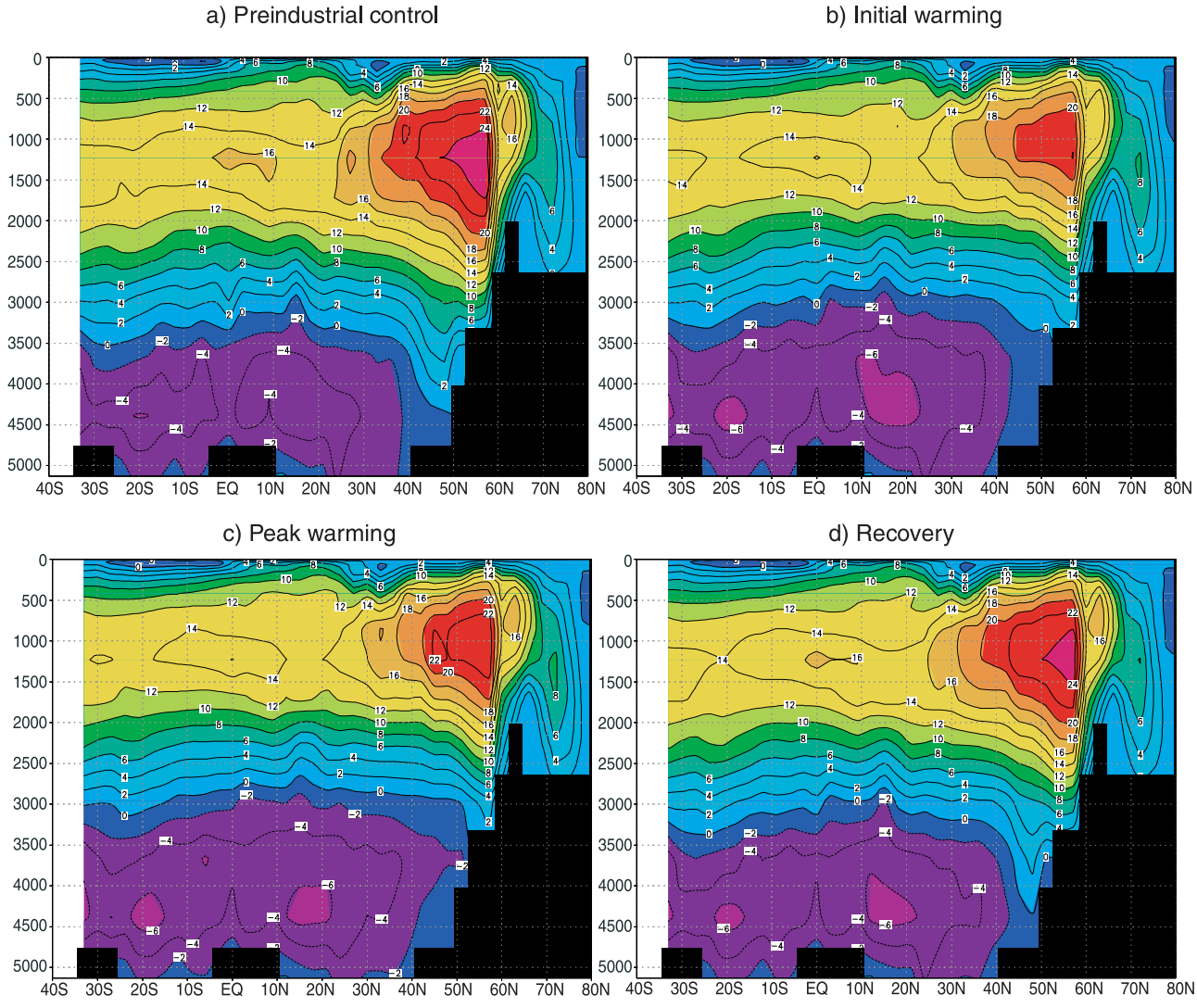

Figure 6. Latitude-depth distributions of the annual mean meridional overturning stream function in the Atlantic Ocean for four different phases of the experiment: (a) preindustrial control, (b) initial warming (year 250), (c) peak warming (year 1000), and (d) recovery phase (year 2500). Contour interval is 2 Sv. Flow is positive along positive contours.

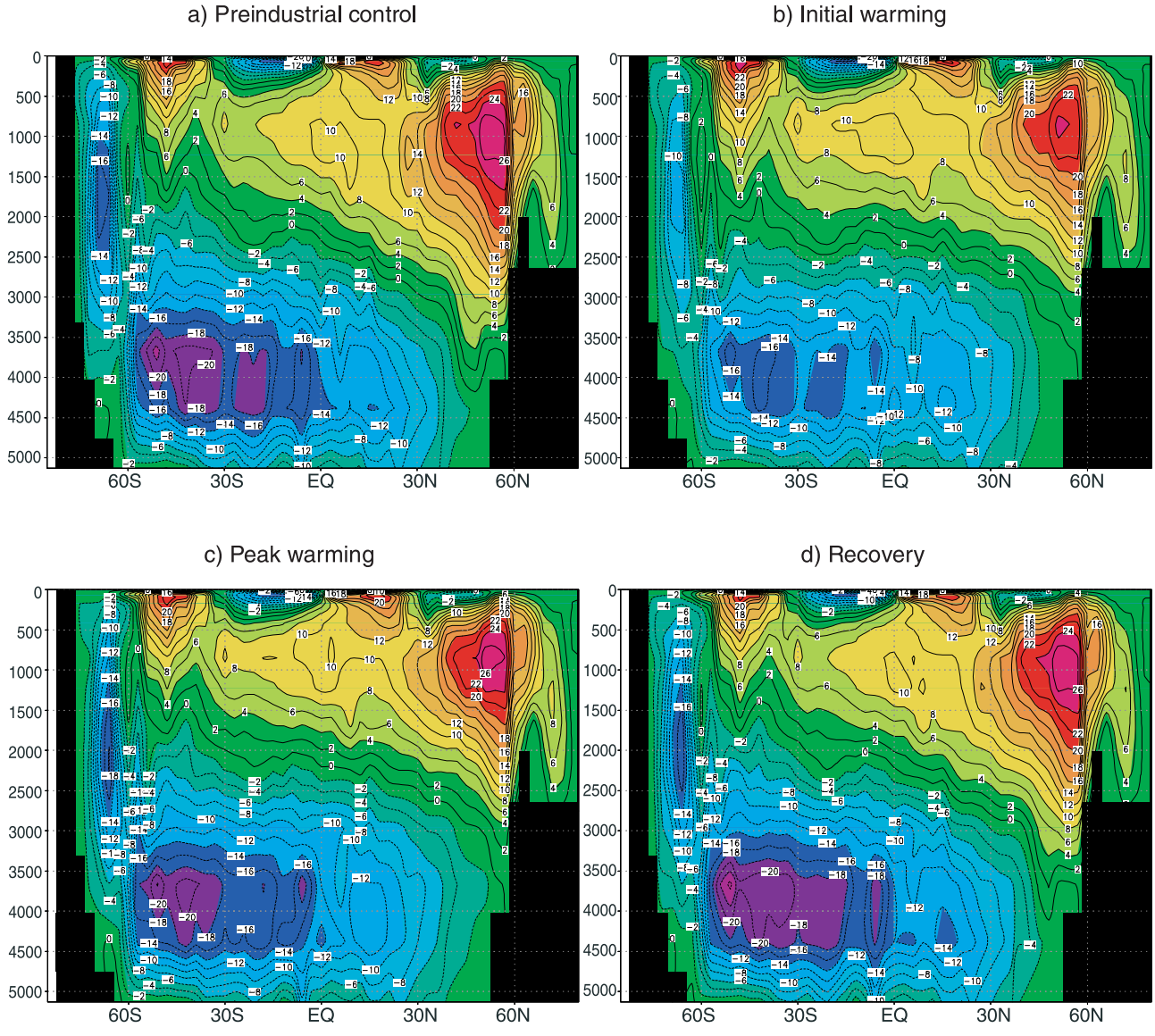

Figure 8. Latitude-depth distributions of the annual mean meridional overturning stream function in the global ocean for four different phases of the experiment: (a) preindustrial control, (b) initial warming (year 250), (c) peak warming (year 1000), and (d) recovery phase (year 2500). Contour interval is 2 Sv. Flow is positive along positive contours.

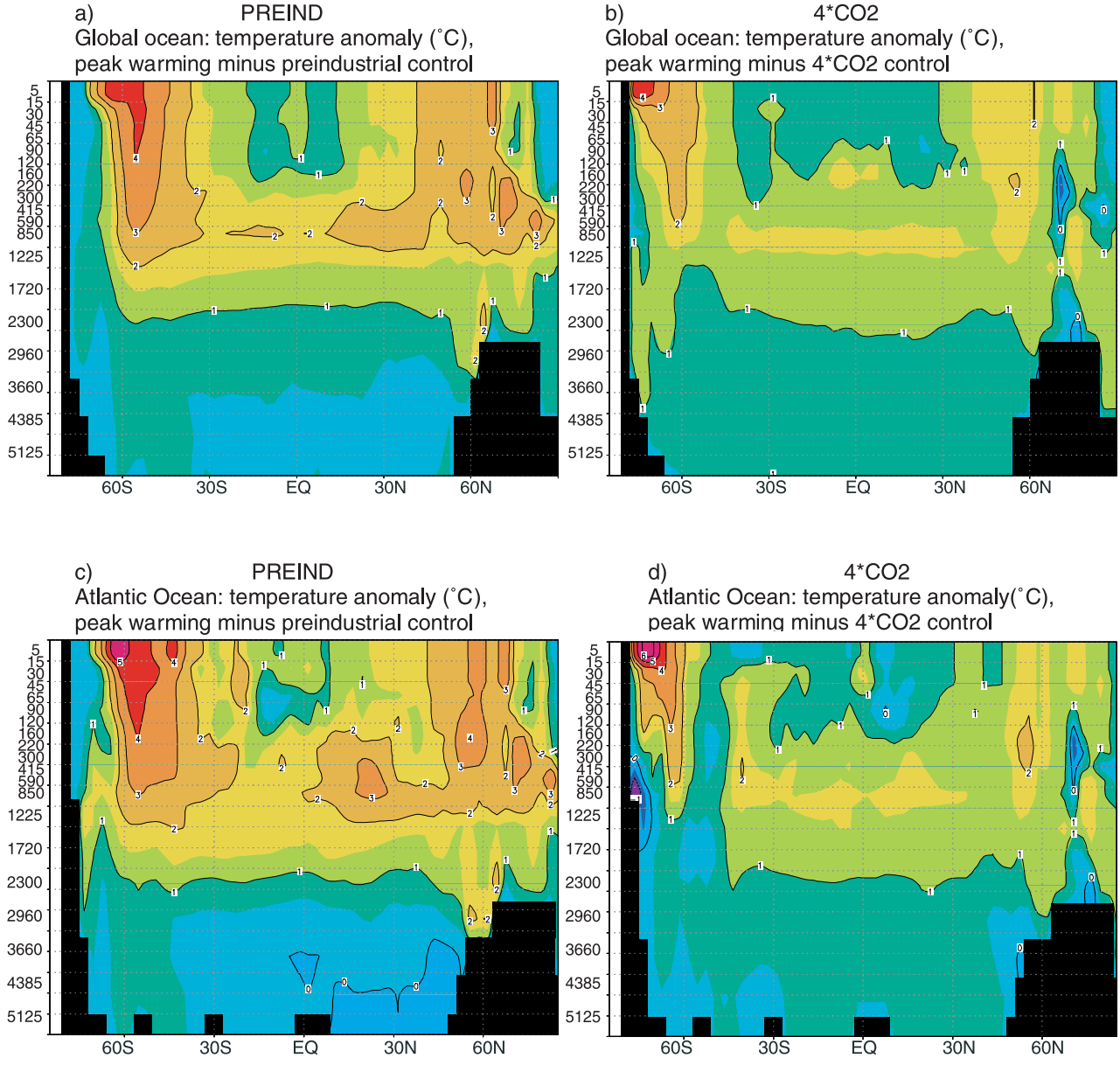

Figure 12. Latitude-depth distribution of the ocean temperature anomaly (°C): peak warming (year 1000) minus reference climate: (a) global ocean PREIND, (b) global ocean 4*CO_2, (c) Atlantic Ocean PREIND, and (d) Atlantic Ocean 4*CO_2.